Molecular Therapy
Original Article

Improved CoChR Variants Restore Visual Acuity and Contrast Sensitivity in a Mouse Model of Blindness under Ambient Light Conditions

Tushar H. Ganjawala,[1] Qi Lu,[1] Mitchell D. Fenner,[1] Gary W. Abrams,[1] and Zhuo-Hua Pan[1]

[1]Department of Ophthalmology, Visual and Anatomical Sciences, Kresge Eye Institute, Wayne State University School of Medicine, Detroit, MI, USA

Severe photoreceptor cell death in retinal degenerative diseases leads to partial or complete blindness. Optogenetics is a promising strategy to treat blindness. The feasibility of this strategy has been demonstrated through the ectopic expression of microbial channelrhodopsins (ChRs) and other genetically encoded light sensors in surviving retinal neurons in animal models. A major drawback for ChR-based visual restoration is low light sensitivity. Here, we report the development of highly operational light-sensitive ChRs by optimizing the kinetics of a recently reported ChR variant, *Chloromonas oogama* (CoChR). In particular, we identified two CoChR mutants, CoChR-L112C and CoChR-H94E/L112C/K264T, with markedly enhanced light sensitivity. The improved light sensitivity of the CoChR mutants was confirmed by *ex vivo* electrophysiological recordings in the retina. Furthermore, the CoChR mutants restored the vision of a blind mouse model under ambient light conditions with remarkably good contrast sensitivity and visual acuity, as evidenced by the results of behavioral assays. The ability to restore functional vision under normal light conditions with the improved CoChR variants removed a major obstacle for ChR-based optogenetic vision restoration.

INTRODUCTION

Severe photoreceptor cell death in patients with inherited or acquired retinal degenerative diseases, such as retinitis pigmentosa (RP) and age-related macular degeneration (AMD), often leads to partial or complete blindness.[1,2] Optogenetics employing the ectopic expression of genetically encoded light sensors to impart light sensitivity to surviving retinal neurons has the potential to restore significant useful vision to blind individuals.[3–5] The feasibility of this strategy has been demonstrated using microbial channelrhodopsins (ChRs), particularly ChR2, and other optogenetic tools in animal models.[6–18] The use of ChRs as optogenetic tools for vision restoration has several advantages. First, all microbial rhodopsins use all-*trans* retinal as a chromophore, which is present in our body fluids.[19] Therefore, an exogenous supply of the chromophore is not required. Second, ChRs are light-gated channels that represent a direct way to manipulate the membrane excitability of neurons.[20,21] Moreover, ChRs with different biophysical properties, such as channel kinetics, ionic selectivity, and spectral sensitivity, that are either found in nature or generated by molecular engineering are becoming increasingly available;[22–33] thus, ChRs represent a versatile set of tools with the potential to restore complex visual processing features in the degenerated retina.[34–36]

However, a major drawback for using ChR2 in particular, and ChRs in general, for vision restoration is their low light sensitivity.[3,4,6] Although more light-sensitive ChR variants have been reported and used to restore vision, all previous reports of ChR-based vision restoration employed light intensities that were substantially greater than normal lighting levels.[12,18,37,38] The requirement for a high light intensity to activate ChRs could constrain the practical applications in vision restoration, and it has also raised concerns regarding phototoxicity to retinal tissues. For the latter, efforts have been attempted to use ChRs with red-shifted spectra to mitigate the phototoxicity, because a longer wavelength light has higher intensity tolerance for phototoxicity.[18] Furthermore, the lack of efficient optogenetic tools that are activated under normal light conditions has limited the ability to evaluate the optogenetically restored visual functions. Thus, the development of more light-sensitive ChRs is highly desired.

The operational light sensitivity (hereafter referred to as light sensitivity) of a ChR can be improved by prolonging its deactivation, or off rate,[39] albeit through a trade-off between light sensitivity and temporal kinetics. Since vision restoration could tolerate relatively slow kinetics, we have previously used this strategy to develop more light-sensitive ChR2 mutants by optimizing its kinetics.[30] Specifically, retinal ganglion cells (RGCs) expressing a more light-sensitive ChR2 mutant, ChR2-L132C/T159S, with an off rate of ~1 s, can follow flickering light stimuli up to at least 10 Hz, which should still provide a useful temporal resolution considering the fusion frequency to flickering stimuli for human rod vision is ~15 Hz.[40]

To develop more light-sensitive ChRs with this strategy would be to use more efficient ChR variants. Recently, a new blue light-sensitive

Received 8 January 2019; accepted 3 April 2019;
https://doi.org/10.1016/j.ymthe.2019.04.002.

Correspondence: Zhuo-Hua Pan, PhD, Department of Ophthalmology, Visual and Anatomical Sciences, Kresge Eye Institute, Wayne State University School of Medicine, 540 E. Canfield Avenue, Detroit, MI 48201, USA.
E-mail: zhpan@med.wayne.edu

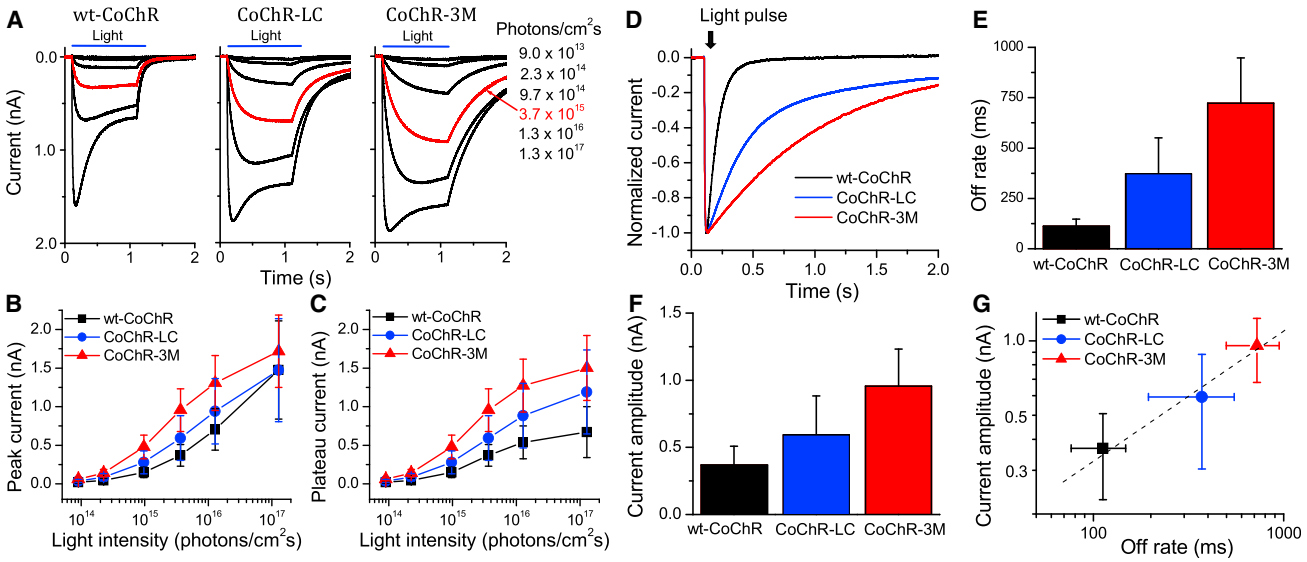

Figure 1. Light Intensity and Response Properties of wt-CoChR and Its Two Mutants, CoChR-LC and CoChR-3M, in HEK Cells

(A) Representative light-evoked current traces in voltage-clamp recordings. The currents were evoked by 1-s light pulses at 480 nm with incrementally increasing light intensities measured as photons/cm^{2}s. The red current traces were elicited by light with an intensity of 3.7 × 10^{15} photons/cm^{2}s. (B and C) The light intensity and current response relationships were measured at the peak (B) and plateau (C) currents. (D) Representative current decay traces elicited by a 10-ms light pulse at the light intensity of 8.9 × 10^{17} photons/cm^{2}s were used to compare the deactivation kinetics. (E) Average values for deactivation time constants or off rates. The off rates were obtained by fitting a single exponential function to the decaying phase of the currents. (F) Average peak currents elicited at the light intensity of 3.7 × 10^{15} photons/cm^{2}s. (G) Plot of the current amplitudes and the off rates. The current amplitudes and off rates for CoChRs exhibit a linear correlation. All data are presented as means ± SD (n = 10 cells).

ChR variant, *Chloromonas oogama* (CoChR), was reported to show good membrane expression and large photocurrent but a relatively fast off rate.[31,41,42] In this study, we report the development of CoChR mutants with improved light sensitivity by optimizing the off rate through site-directed mutagenesis. The expression of the optimized CoChR mutants restores functional vision in a blind mouse model under ambient light conditions.

RESULTS

The Development of Optimized CoChR Mutants for Vision Restoration

Semi-rational site-directed mutagenesis was performed on CoChR at the sites C108, L112, D136, T139, K264, and H94 to alter its off rate (Figure S1). C108, L112, D136, and T139 were chosen because they correspond to the C128, L132, D156, and T159 of ChR2, and mutations at these sites have previously been shown to alter the off rate of ChR2.[26–28,30,43,44] K264 was chosen to disrupt a potential endoplasmic reticulum-retrieval signal, "KK^{264}XX," which may affect intracellular trafficking.[45] The H94 site corresponds to the amino acid that has been proposed to influence ion transport activity in anion ChR2.[46] The mutants were first screened for intracellular protein trafficking and membrane expression efficiency based on GFP expression in HEK cells.[30] Mutants that exhibited good or relatively good membrane expression were further examined for their light response properties, i.e., spectral sensitivity, current amplitude, and off rate. None of the examined mutants exhibited a significant change in spectral sensitivity (Figure S2). The off rate and current amplitude were subsequently examined at 480 nm.[31,42] The current amplitudes and off rates for the examined mutants are shown in Table S1.

Two mutants, CoChR-L112C (CoChR-LC) and CoChR-H94E/L112C/K264T (CoChR-3M) with representative ranges of off rates, 372 and 723 ms, respectively, together with wild-type (wt)-CoChR (off rate: 112 ms), which are referred to as CoChRs hereafter, were selected for further investigations. The membrane expression efficiencies of these two mutants were comparable to wt-CoChR, as assessed by GFP fluorescence intensity in the plasma membrane (Figure S3). Figure 1 shows light-elicited currents in response to incrementally increasing light intensities (Figure 1A) and the light intensity-response curves measured at current peak (Figure 1B) and plateau (Figure 1C). The current amplitudes for the two mutants, particularly CoChR-3M, evoked by relative low intensities of light were much larger than wt-CoChR, as evidenced by a comparison of the red traces elicited by light with an intensity of 3.7 × 10^{15} photons/cm^{2}s. When the current off rates (Figures 1D and 1E) were plotted against the current amplitude (Figure 1F), the increased current amplitudes for the mutants were correlated with the increased off rates (Figure 1G). Additionally, for both mutants, the current desensitization during high-intensity light stimulation was markedly reduced (see Figure 1A).

Long-Term Stable Expression of CoChRs in the Retina *In Vivo*

We next evaluated the expression of CoChRs in the mouse retina *in vivo*. The adeno-associated virus (AAV) serotyp 2 vectors carrying

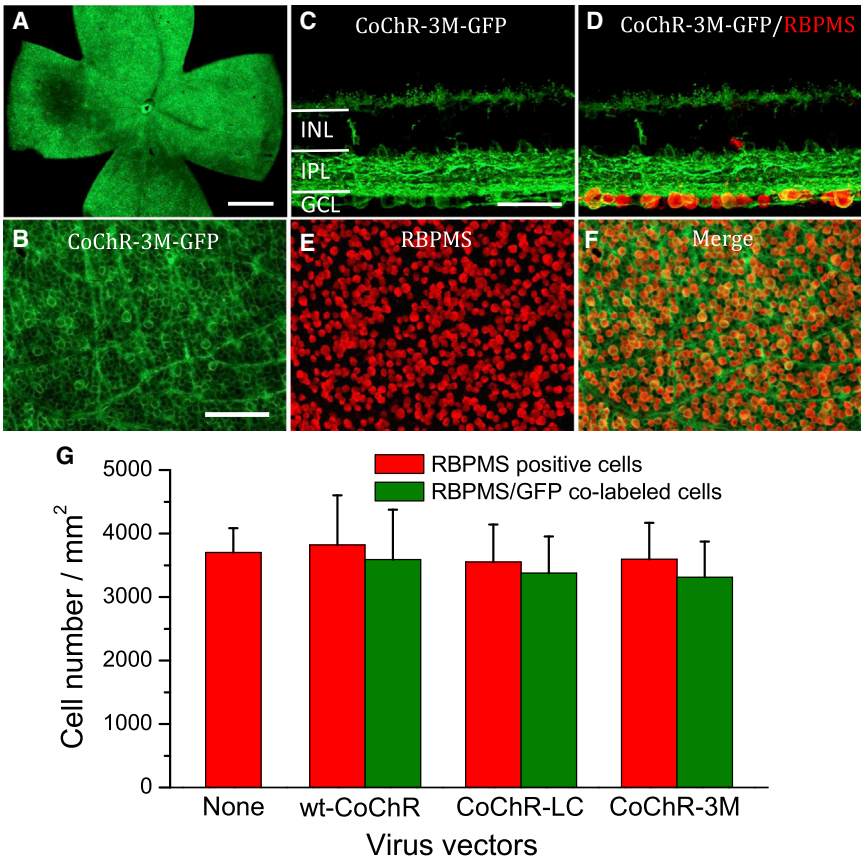

Figure 2. Expression of CoChR-GFP in TKO Mouse Retinas *In Vivo*

(A and B) Representative immunofluorescence images of CoChR-3M-GFP in retinal whole mounts at low (A) and high magnification (B). (C–F) Co-labeling of GFP with RBPMS, an RGC-specific marker, in retinal vertical sections (C and D) and in retinal whole mounts (B, E, and F). (G) The density of RGCs in control retinas and CoChR-treated retinas was assessed by immunolabeling for RBPMS (red). The data are presented as means ± SD (n = 4 retinas). 94%, 95%, and 92% of RGCs in wt-CoChR-, CoChR-LC-, and CoChR-3M-treated retinas were co-labeled with GFP, respectively. The densities of RGCs were not significantly different between control and treated retinas for all three CoChRs ($p > 0.05$; one-way ANOVA). The results were obtained from the mice 6 months after virus vector injection. Scale bars, 500 μm (A), 50 μm (C and D), and 100 μm (B, E, and F).

the CoChR-GFP transgenes, under the control of the CAG promoter, were intravitreally injected in the eyes of two mouse models, wild-type C57BL/6J mice and a blind Opn4$^{-/-}$Gnat1$^{-/-}$Cnga3$^{-/-}$ triple knockout (TKO) transgenic mouse line. The TKO mice were chosen because they lack an optomotor response (OMR), pupillary constriction, and apparent photoreceptor death.[38,47] Thus, the use of this mouse line enables the assessment of the restoration of visual function by optomotor behavioral assays without the confounds of complications caused by melanopsin-mediated papillary constriction and severe photoreceptor death.

The expression pattern in the retina was the same for all three CoChRs in both mouse lines, as shown in representative images for CoChR-3M in retinal whole mounts (Figures 2A and 2B; Figure S4) and in retinal vertical sections (Figure 2C) for TKO mice. Based on co-labeling with an anti-RNA-binding protein with multiple splicing (RBPMS) antibody, an RGC-specific marker, the expression of CoChR-GFP was predominantly observed in RGCs, along with some amacrine and horizontal cells (Figures 2C and 2D). Based on co-labeling with RBPMS in retinal whole mounts (Figures 2B, 2E, and 2F; Figure S4), more than 90% (94%, 95%, and 92% for wt-CoChR, CoChR-LC, and CoChR-3M, respectively) of RGCs were transduced by CoChR-GFP (Figure 2G). The density of RGCs was not significantly different compared to the control for all three vector-treated mice examined 6 months after virus vector injection (Figure 2G), suggesting CoChRs did not cause significant long-term toxicity *in vivo*.

Light Response Properties Assessed Using MEA Recordings

We next examined the light sensitivity of the CoChR-expressing RGCs by performing multi-electrode array (MEA) recordings from retinal whole mounts of both C57BL/6J and TKO mice. For C57BL/6J mice, the photoreceptor-mediated light responses were blocked with a mixture of antagonists, i.e., 6-cyano-7-nitroquinoxaline-2,3-dione (CNQX, 50 μM), D(−)-2-amino-5-phosphonopentanoic acid (D-AP5, 20 μM), L-(+)-2-amino-4-phosphonobutyric acid (L-AP4, 20 μM), ACET (2 μM), dihydro-β-erythroidine (DHβE, 20 μM), bicuculline (50 μM), and strychnine (5 μM). For TKO mice, no photoreceptor-mediated light response was observed under our light-adapted conditions; nevertheless, L-AP4 (20 μM) and ACET (2 μM) were used in some recordings. No differences were observed between C57BL/6J and TKO mice and among TKO mice with and without the application of L-AP4 and ACET, and, therefore, the results were combined.

We first examined the action spectrum of CoChR-LC and CoChR-3M based on the CoChR-mediated spiking activities elicited by 1-s light pulses of different wavelengths with a 2.0-neutral density (ND) filter (Figure 3A). The peak spectra for both mutants were around 460–470 nm after being normalized to equal photon fluxes (Figure 3B).

We next examined the light sensitivity of CoChR-mediated spiking activities elicited by 1-s light pulses at 480 nm with incrementally increasing light intensities adjusted with ND filters. Figure 4 shows representative recordings (Figure 4A) and the normalized distributions of RGCs versus threshold light intensities (Figure 4B). For

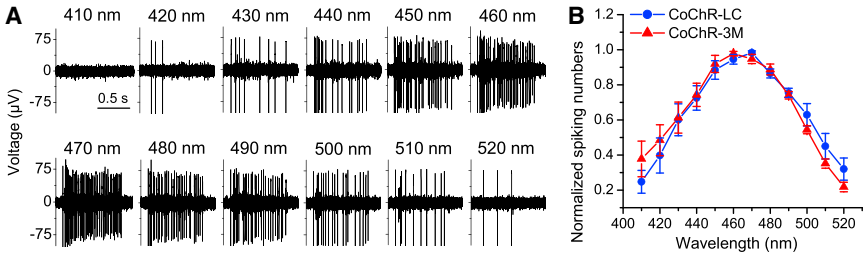

Figure 3. Multielectrode Array Recordings of RGCs from Retinal Whole Mounts for Assessing the Action Spectrum of CoChR Mutants

(A) Representative recordings of CoChR-mediated spiking activities in CoChR-LC-treated retinas. The spiking activities were elicited by 1-s light pulses with the wavelengths from 410 to 520 nm with an ND filter of 2.0. (B) The spectral curves for CoChR-LC (n = 5 cells) and CoChR-3M (n = 5 cells) after being normalized to equal photon fluxes. The data are presented as means ± SD.

CoChR-3M, the threshold light intensity for the most light-sensitive RGCs was at 4.0 ND (~1.9×10^{12} photons/cm^{2}s) and for the highest number of activated RGCs was at 3.0 ND (~2.0×10^{13} photons/cm^{2}s). The distribution curves for CoChR-LC and wt-CoChR were shifted approximately 0.5 and 1 log unit toward a higher light intensity, respectively (Figure 4B). Thus, the MEA recordings confirmed the subsequent improvement in the light sensitivity of CoChR-LC and CoChR-3M compared with wt-CoChR.

We further examined the temporal coding ability of CoChR-expressing RGCs. For this purpose, the spiking activity of RGCs in CoChR-treated retinas was examined in response to flickering stimuli of different frequencies. Figure 5 shows representative recordings (Figures 5A–5C) and frequency-dependent response attenuation curves (Figure 5D). For CoChR-3M and CoChR-LC, the estimated cutoff or corner frequencies, which were defined at an attenuation of −3 dB, were ~13 and ~20 Hz, respectively.

Assessing CoChR-Restored Visual Functions by Optomotor Assays

The restoration of the visual function of TKO mice with CoChRs was further assessed using optomotor behavioral assays. The experiments were first conducted using a homemade optomotor system (Figure 6A) with blue light-emitting diodes (LEDs) (a peak wavelength at ~470 nm) as light illumination (Figure 6B).[38] The OMR was observed in TKO mice treated with all three CoChRs. Figure 6C shows the relationships between the threshold light intensity and spatial frequency. The threshold light intensity required to evoke the OMR depended on the spatial frequency. The most sensitive frequency was approximately 0.042 cycles/degree (c/d) for all three CoChRs. Consistent with the electrophysiological recordings, CoChR-3M (n = 7) was the most light-sensitive CoChR, followed by CoChR-LC (n = 7) and wt-CoChR (n = 5), as evidenced by a subsequent shift in the curves upward to the higher light intensity. In CoChR-3M-treated mice at the most sensitive spatial frequency (0.042 c/d), the OMR was elicited by a light intensity as low as 6.4×10^{12} photons/cm^{2}s, with an average value of $1.5 \pm 0.76 \times 10^{13}$ photons/cm^{2}s (mean ± SD, n = 7). The frequency-dependent light sensitivity curve for CoChR-3M-treated mice (n = 4) was not significantly changed for up to 12 months (the longest time examined) (Figure 6D).

Since CoChRs are blue light sensitive, we next examined the efficacy of CoChR-3M compared to the red-shifted ChR variants ReaChR[18,29] and Chrimson.[31] Virus vectors carrying ReaChR and Chrimson were constructed using the same virus cassette, and TKO mice were injected with the same amount of virus particles. Figure 6E shows the light intensity and spatial frequency relationships for ReaChR and Chrimson measured with green LEDs (~520 nm) and yellow LEDs (~590 nm) (Figure 6B), which are near the peak wavelength of ReaChR (~530 nm)[18] and Chrimson (~590 nm),[31] respectively. Clearly, CoCh-3M exhibited higher light sensitivity than ReaChR (n = 7) and Chrimson (n = 6) (Figure 6E). In another comparison, we examined the efficacy using natural white LEDs (4,500 K) as light illumination (Figure 6B). Again, CoCh-3M displayed higher light sensitivity than ReaChR (n = 7) and Chrimson (n = 6) (Figure 6F). Strikingly, in CoChR-3M-treated mice, the light intensity required to elicit the OMR up to the spatial frequency of ~0.20 c/d was less than or equal to 50 μW/cm^2 (indicated by the dashed line in Figure 6F). This intensity is roughly equivalent to the light intensity that is produced by a normal 250-nit liquid crystal display (LCD) monitor. Moreover, at the most sensitive spatial frequency (0.042 c/d), the OMR was elicited by the white light with an average intensity of ~10 μW/cm^2 (9.4 ± 12.4 μW/cm^2; mean ± SD, n = 7) (Figure 6F).

CoChRs Restored Visual Acuity and Contrast Sensitivity

Since the OMR in TKO mice treated with CoChR mutants was elicited under ambient light levels, we expected that the OMR would also be elicited in these mice by an LCD monitor-based virtual optomotor system, OptoMotry.[48] The use of OptoMotry enables the examination of contrast sensitivity and a more accurate visual acuity. Indeed, the OMR was observed in both CoChR-LC- and CoChR-3M-treated mice using OptoMotry (Video S1). Figures 7A and 7B show the spatial contrast sensitivities and visual acuities, respectively, for CoChR-3M (n = 8) and CoChR-LC (n = 7). For comparison, the results from sighted C57BL/6J mice are also shown (n = 4). For CoChR-3M-treated mice tested at the most sensitive spatial frequency (0.042 c/d), the highest observed contrast sensitivity was 6.7 (or 15% contrast), with an average value of 4.2 ± 1.8 (mean ± SD; n = 8; Figure 7A); the highest observed visual acuity was 0.24 c/d, with an average value of 0.22 ± 0.02 c/d (mean ± SD; n = 8; Figure 7B). For CoChR-3M-treated mice (n = 4), both the spatial sensitivity curve (Figure 7C) and visual acuity (Figure 7D) were not significantly different between 1 and 12 months after virus injection.

We further examined the temporal tuning properties of CoChR-LC- and CoChR-3M-restored vision. The temporal contrast sensitivities in CoChR-LC- (n = 5) and CoChR-3M-treated mice (n = 5) were

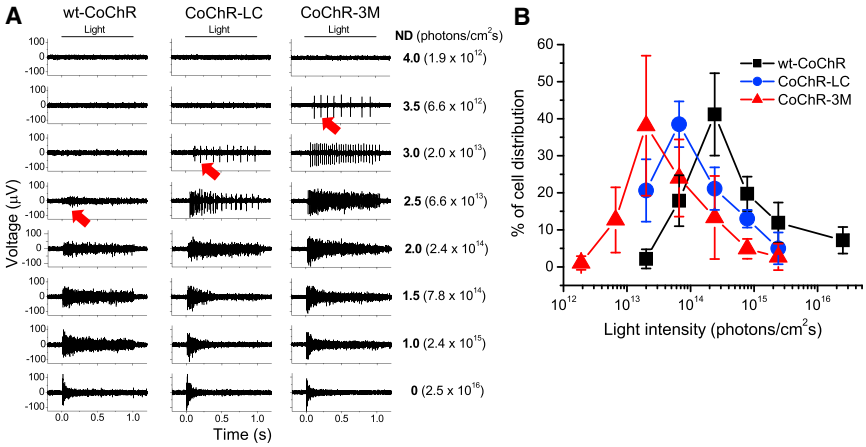

Figure 4. Multielectrode Array Recordings of RGCs from Retinal Whole Mounts for Assessing the Light Sensitivity of CoChRs

(A) Representative recordings of CoChR-mediated spiking activities in wt-CoChR-, CoChR-LC-, and CoChR-3M-treated retinas. The spiking activities were elicited by 1-s light pulses with incrementally increasing light intensities adjusted with neutral density (ND) filters of 4.0, 3.5, 3.0, 2.5, 2.0, 1.5, 1.0, and 0. The light intensities measured as photons/cm^{2}s are also shown. The threshold light intensities required to elicit spiking activities in wt-CoChR-, CoChR-LC-, and CoChR-3M-treated retinas were observed with ND filters of 2.5, 3.0, and 3.5, respectively (marked with arrows). (B) The distributions of the normalized number of RGCs (averaged through the recorded retinas, mean ± SD) versus threshold light intensities for wt-CoChR (4 retinas, 226 cells), CoChR-LC (6 retinas, 299 cells), and CoChR-3M (6 retinas, 319 cells).

examined at their most sensitive spatial frequency (0.042 c/d), with rotation speeds from 1.5 to 50 degrees/s (d/s) (Figure 8A). For comparison, the results from normally sighted C57BL/6J mice (n = 4) examined at the spatial frequency of 0.064 c/d are also shown. The contrast sensitivity functions in CoChR-treated mice exhibited the peak sensitive speed of ~12 d/s, the same as in normally sighted mice (Figure 8A). Figure 8B replotted the data to show the relationships of the contrast sensitivity and temporal frequency. The peak sensitive frequencies for both CoChR-LC and CoChR-3M were at ~0.5 cycles/s (c/s), which was lower than the value of ~0.8 c/s in normally sighted mice. However, no apparent difference in the temporal tuning preference was observed between CoChR-LC and CoChR-3M; but, the contrast sensitivity of CoChR-3M was again significantly higher than CoChR-LC.

DISCUSSION

In this study, we used the strategy of prolonging and optimizing the off rate by employing site-directed mutagenesis to develop ChRs with improved light sensitivity based on the CoChR variant. CoChR was chosen because it exhibits larger photocurrent than ChR2 but still retains relatively fast kinetics or off rate,[31] suggesting that CoChR is more efficient than ChR2, likely due to its intrinsic higher single-channel conductance. We examined two representative CoChR mutants, CoChR-LC and CoChR-3M, by extending its off rate from 112 to 372 and 723 ms, respectively. We showed the enhanced photocurrent for CoChR-L112C and CoChR-3M compared to wt-CoChR using *in vitro* patch-clamp recordings in HEK cells and the enhanced light sensitivity of CoChR-expressing RGCs employing *ex vivo* MEA recordings from the retina. Furthermore, we showed the improved light sensitivity of these two CoChR mutants by OMR behavioral assessments in TKO mice. For the most light-sensitive CoChR mutant, CoChR-3M, OMR at the spatial frequency of 0.042 c/d was elicited by a light intensity as low as 6.4×10^{12} photons/cm^{2}s, with an average intensity of $1.5 \pm 0.76 \times 10^{13}$ photons/cm^{2}s. Moreover, in the CoChR-3M-treated mice, the light intensity required to elicit the OMR over its whole effective frequency falls within the ambient lighting level, which can be generated with a normal LCD monitor. To our knowledge, this study is the first to show that ChR-mediated restoration of vision functions is achieved under ambient light conditions.

As we previously reported,[38] there is a difference in the threshold light sensitivities required to elicit responses between MEA recordings and OMR measurements. For example, in CoChR-3M-treated mice, the lowest light intensity (2×10^{12} photons/cm^{2}s; see Figure 4B) required to evoke RGC activities was ~3 times lower than the lowest light intensity (6.4×10^{12} photons/cm^{2}s) to elicit OMR but ~1 log unit lower than the average light intensity ($1.5 \pm 0.76 \times 10^{13}$ photons/cm^{2}s) to elicit OMR. The latter, however, is comparable to the intensity (2×10^{13} photons/cm^{2}s) required to evoke the peak number of RGC activities. Therefore, the difference is likely in part due to the requirement of above-threshold RGC activities to drive the OMR. In addition, the light intensity in MEA recordings was measured at the level of the retina, while the light intensity in the behavioral testing was measured on the surface of the eye. The attenuation of light intensity through the eye would also contribute to the difference.

Based on the OMR assessment, the light sensitivity of CoChR-3M is approximately 1 log unit higher than the previously optimized ChR2 mutant, ChR2-L112C/T159S, and nearly 3 log units higher than wt-ChR2.[38] CoChR-3M is also more sensitive than the currently available red-shifted ChRs, ReaChR and Chrimson. Under the same experimental conditions, the light intensity required to elicit the OMR in mice expressing CoChR-3M is at least 1 and 2 log units less than ReaChR and Chrimson, respectively, compared either at their peak-sensitive wavelengths or with natural white-light LEDs. The use of the red-shifted ChRs for vision restoration was aimed at increasing the light intensity tolerance and preventing potential phototoxicity to retinal tissues.[18] Although CoChRs are sensitive to blue light, since the operational light intensity for the CoChR mutants, particularly CoChR-3M, is within normally encountered levels, the phototoxicity for the use of CoChR-3M for vision restoration should no longer be an issue.

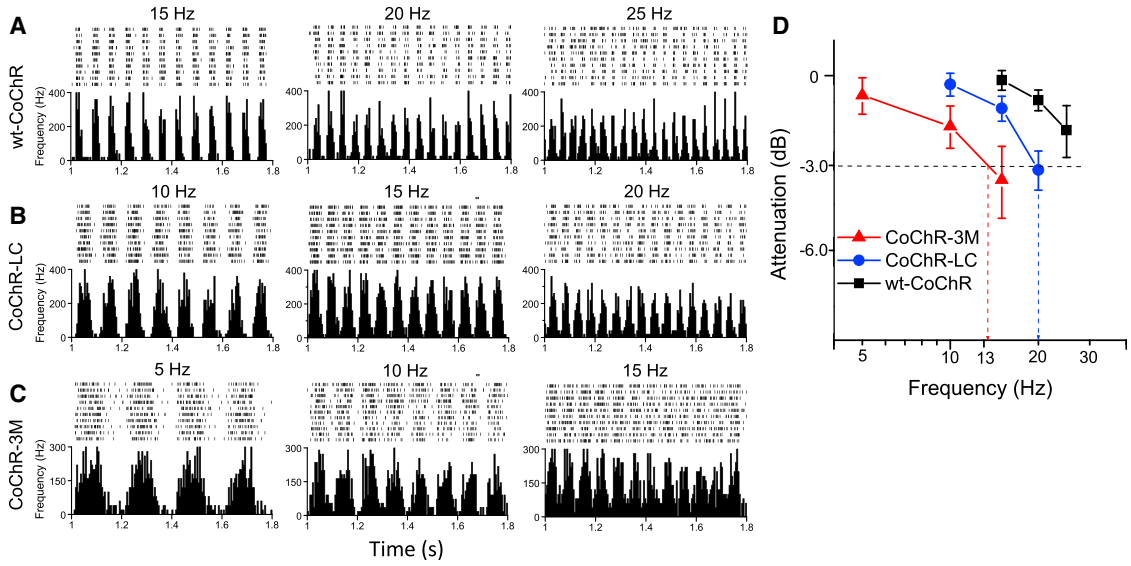

Figure 5. Multielectrode Array Recordings of RGCs for Assessing the CoChR-Mediated Temporal Dynamics

(A–C) Representative recordings of CoChR-mediated spiking activities in wt-CoChR- (A), CoChR-LC- (B), and CoChR-3M-treated retinas (C) in response to flickering stimuli with three different frequencies. A raster plot of 10 recordings (top) and an average spike rate histogram (bottom) are shown. The light intensities used were adjusted with a 1.5-ND filter for wt-CoChR (A) and a 2.0-ND filter for both CoChR-LC (B) and CoChR-3M (C). (D) The frequency-dependent response-amplitude-attenuation curves for wt-CoChR, CoChR-LC, and CoChR-3M. The attenuation is shown in decibels (dB). The horizontal dashed line indicates the −3-dB attenuation. The cutoff or corner frequencies were estimated to be 13 and 20 Hz for CoChR-3M and CoChR-LC, respectively, as indicated by the vertical dashed lines. The data are presented as means ± SD for wt-CoChR (n = 10 cells), CoChR-LC (n = 9), and CoChR-3M (n = 14).

It should be mentioned that there is a difference in the transmission of short wavelengths through cornea and lens between mice and humans, because the cutoff frequency for mice is around 310 nm, whereas for humans it is around 390 nm.[49–51] Although the action spectra of CoChRs largely fall in the range greater than 400 nm, the effective solar or artificial light intensity for CoChRs could still be more attenuated in humans than in mice. Therefore, further development of highly light-sensitive and red-shifted ChRs would be more ideal.

The restoration of functional vision in this study was assessed in a TKO mouse model by taking advantage of its unique properties of the lack of the OMR, melanopsin-mediated pupillary constriction, and apparent death of photoreceptor cells.[38,47] Therefore, ChR-mediated light sensitivity was assessed under the condition without attenuation by melanopsin-mediated pupillary constriction. In addition, the lack of apparent photoreceptor degeneration in TKO mice provides a condition to evaluate the restoration of visual functions without the confounds of complications caused by severe retinal remodeling in animal models of severe photoreceptor degeneration. Consistently, our results showed that the restored visual functions, such as light sensitivity, contrast sensitivity, and visual acuity, were stable for up to at least 1 year in TKO mice. Thus, the TKO mice represent a unique model for assessing the efficacy of optogenetic tools and different treatment strategies.[38]

The development of highly light-sensitive CoChR mutants combined with the use of the TKO mice allowed us to quantitatively assess the properties of optogenetically restored vision. First, CoChR-3M-treated TKO mice achieved an average visual acuity of 0.22 c/d. This value is remarkably good in comparison to the value of ~0.40 c/d observed in normally sighted mice.[45] The lower visual acuity for the ChR-restored vision in TKO mice than in normally sighted mice is expected and likely due to the larger ChR-mediated receptive fields of RGCs than their intrinsic receptive fields. Therefore, further studies would be interesting to determine whether the restored visual acuity could be improved by reducing ChR-mediated receptive fields, such as by subcellular targeting.[35,36]

Furthermore, both the spatial and temporal contrast sensitivity functions in CoChR-treated mice exhibit a characteristic band-pass shape.[52] The most sensitive spatial and temporal frequencies for both mutants are at ~0.042 c/d and ~0.5 c/s, respectively. These values are only moderately lower than those observed in normally sighted mice. Specifically, at the most sensitive spatial frequency of 0.042 c/d, the CoChR-3M-treated TKO mice exhibited contrast sensitivity up to 6.7 (or 15% contrast), with an average value of 4.2. This value is also remarkably good compared with the value of ~10–25 (4%–10% contrast) in normally sighted mice (Figure 6A).[45] Because ChR expression was achieved by predominantly targeting the ChRs to RGCs in this study, the ability to restore contrast sensitivity is even surprising, because the contrast sensitivity is known to be mediated by surround inhibition in the retina.[53,54] It is possible that the surround inhibition is generated by the inhibitory inputs from ChR-expressing amacrine cells (see Figure 2D). Further studies

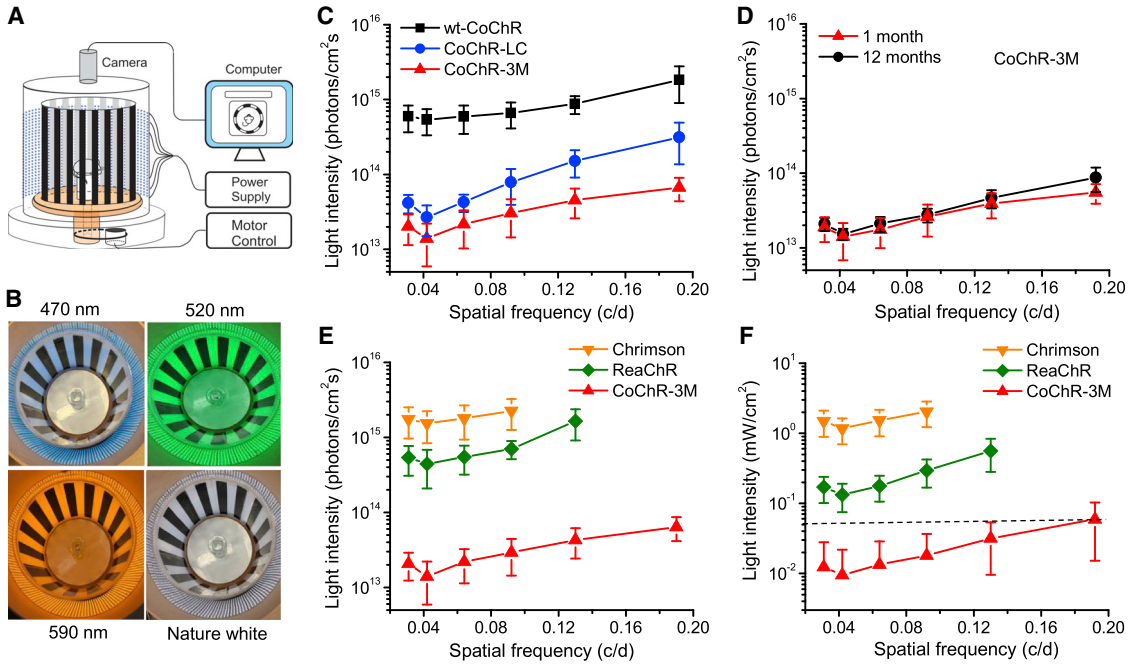

Figure 6. Properties of the OMR in TKO Mice Mediated by CoChRs and Red-Shifted ChRs

(A and B) A homemade optomotor system (A) that uses blue (470 nm), green (520 nm), yellow (590 nm), or natural white-light (4,500 K) LEDs as the light illumination source (B). (C) The spatial frequency-dependent threshold light intensity curves for wt-CoChR- (n = 5), CoChR-LC- (n = 7), and CoChR-3M-treated mice (n = 7). The OMR was elicited by blue LEDs. (D) The light intensity curves for CoChR-3M-treated mice (n = 4) measured 1 and 12 months after virus vector injection. (E) Comparison of the frequency-dependent threshold light intensity curves for CoChR-3M- (the same data from C), ReaChR- (n = 7), and Chrimson-treated mice (n = 6). The OMR for ReaChR- and Chrimson-treated mice was elicited by green and yellow LEDs, respectively. (F) The frequency-dependent threshold light intensity curves for CoChR-3M- (n = 7), ReaChR- (n = 7), and Chrimson-treated mice (n = 6) elicited with natural white LEDs as the light illumination source. The dashed line estimates the light intensity level produced by a normal LCD monitor. All data are presented as means ± SD from the indicated number of animals.

should be directed at investigating the underlying mechanism(s) and developing better strategies to improve the restored vision.

In addition, although CoChR-3M has slower kinetics than CoChR-LC, no significant difference in the temporal tuning between these two mutants was observed. On the other hand, the overall contrast sensitivity in CoChR-3M-treated mice is significantly higher than in CoChR-LC-treated mice. Our results thus indicate the light sensitivity of optogenetic tools is more critical than kinetics for vision restoration, at least for the range of the kinetics examined in this study.

Optogenetic restoration of vision under ambient light conditions has only been previously reported using G-protein-coupled receptors (GPCRs), such as melanopsin,[8] mammalian rhodopsins,[15,16] and a melanopsin/mGluR6 chimera (Opto-mGluR6).[17] In general, a drawback with the use of GPCRs is their slow kinetics.[55] Other concerns regarding the use of photoreceptor opsins include the availabilities of both the 11-*cis* retinal chromophore and efficient downstream signaling machineries in inner retinal neurons. Surprisingly, vision restoration mediated by the expression of mammalian rhodopsins in RGCs and bipolar cells was reported without an exogenous supply of chromophore *in vivo*.[15,16] The restoration of both visual acuity and contrast sensitivity using mammalian rhodopsin was also reported, particularly through bipolar cell targeting.[16] The use of Opto-mGluR6 targeted to ON bipolar cells is particularly appealing because it utilizes the downstream signaling cascade for mGluR6 receptors in ON bipolar cells.[17] The restoration of a visual acuity of 0.17 c/d was reported with Opto-mGluR6 targeted to retinal ON bipolar cells; but, this was only achieved in a transgenic mouse model. Further studies to compare the efficacy and properties between the improved ChR- and GPCR-based optogenetic tools would be interesting.

In summary, in this study, we developed ChRs with much improved light sensitivity for vision restoration by optimizing the kinetics of CoChR. Functional vision was restored in a blind mouse model under ambient light conditions. Furthermore, the mice with restored vision through predominant RGC targeting exhibit remarkably good contrast sensitivity and visual acuity. The development of the improved CoChR mutants that restore functional vision under normal light conditions removed a major obstacle for the use of ChR-based optogenetic tools to treat blindness.

MATERIALS AND METHODS

DNA Constructs and Viral Vectors

The codon-optimized CoChR, ReaChR, and csChrimson (referred to as Chrimson) were synthesized (GenScript, Piscataway, NJ)

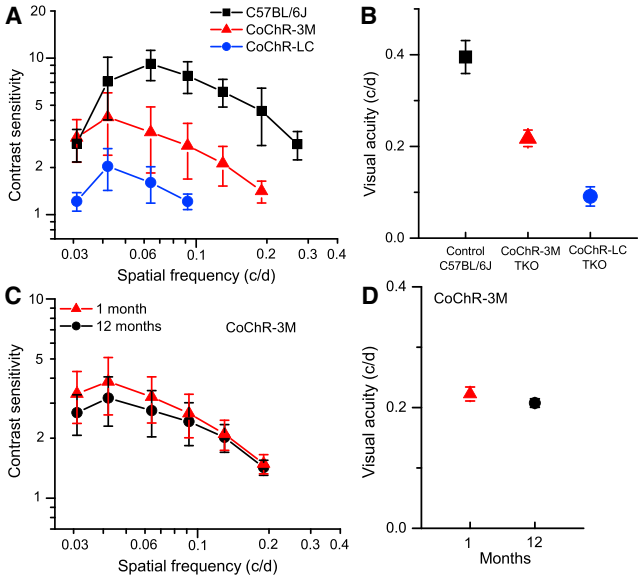

Figure 7. Properties of Spatial Contrast Sensitivity and Visual Acuity in CoChR-Treated TKO Mice Assessed by OptoMotry

(A and B) The spatial frequency-dependent contrast sensitivity curves (A) and visual acuity (B) of CoChR-3M- (n = 8) and CoChR-LC-treated mice (n = 7). For comparison, the contrast sensitivity curve and visual acuity of normally sighted C57BL/6J mice (n = 4) were also measured. (C and D) The contrast sensitivity curves (C) and visual acuity values (D) measured at 1 and 12 months after virus injection for CoChR-3M-treated mice (n = 4). The values for the contrast sensitivity at all spatial frequencies and the values for visual acuity were not significantly different ($p > 0.05$; one-way ANOVA) between 1 and 12 months. All the data are presented as means ± SD from the indicated number of animals.

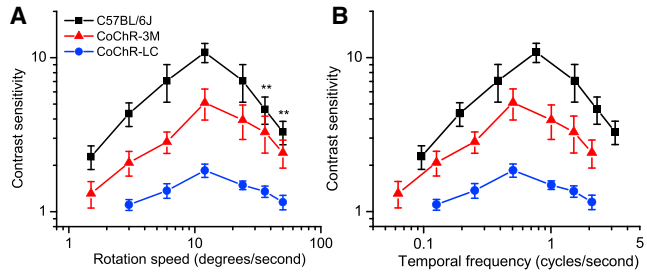

Figure 8. Temporal Tuning Properties of CoChR-Treated TKO Mice Assessed by OptoMotry

(A) The temporal tuning curves in CoChR-LC- (n = 5) and CoChR-3M-treated mice (n = 5) at the spatial frequency of 0.042 c/d with rotation speeds up to 50 d/s. For comparison, the temporal tuning curve for normally sighted C57BL/6J mice (n = 4) at the spatial frequency of 0.064 c/d was also measured. (B) The data were replotted to show the relationships of the contrast sensitivity and temporal frequency (temporal frequency = spatial frequency × rotation speed). All the data points between C57BL/6J and CoChR-3M-treated mice are significantly different. **$p < 0.01$ and $p < 0.001$ for all other data points (one-way ANOVA). The data are presented as means ± SD from the indicated number of animals.

according to the reported amino acid sequences.[29,31] CoChR mutants were generated using site-directed mutagenesis (Agilent Technologies, Santa Clara, CA). CoChR or CoChR mutants were cloned into the recombinant AAV (rAAV) vector cassette and fused in frame to GFP (CoChR-GFP); expression was driven by a CAG (a hybrid cytomegalovirus [CMV] early enhancer/chicken β-actin) promoter, as previously reported.[6,30] Viral vectors were packaged into AAV2/2 serotype for all ChRs and the AAV2.7m8-Y444F capsid variant also for CoChR-L112C and CoChR-3M, and affinity purified by Virovek (Hayward, CA, USA). No differences were observed in the expression and function in mice between the two capsids. Therefore, the results are not differentiated.

HEK Cell Culture, DNA Transfection, Fluorescence Measurements, and Patch-Clamp Recordings

HEK293F cells were maintained in Advance Dulbecco's minimum essential medium (Life Technologies, Grand Island, NY, USA) supplemented with 5% fetal bovine serum, 1× minimum essential medium (MEM) non-essential amino acid solution, 100 U/mL penicillin G, and 100 μg/mL streptomycin at 37°C in a humidified atmosphere of 95% air and 5% CO_2. In preparation for DNA transfection, cells were seeded in 35-mm dishes and transfected with rAAV2 DNA vectors carrying CoChRs using Lipofectamine 2000 (Life Technologies). All-*trans* retinal (1 μM) was added to the culture media at the time of DNA transfection. The procedures for the membrane fluorescence measurements were previously described.[30] Briefly, HEK cells were fixed with 4% paraformaldehyde. Images were taken under fixed light intensity and exposure time using a Zeiss Apotome 2 Optical Photomicroscope (Carl Zeiss Microscopy, Jena, Germany). The fluorescence intensity of each HEK cell was calculated by dividing the total fluorescence value in its plasma membrane region by the total number of pixels of the same region.

Patch-clamp recordings were performed 2 days after DNA transfection. Recordings in the whole-cell configuration were made using standard procedures at room temperature (~22°C). The extracellular recording solution contained the following (in mM): 138 NaCl, 1 $NaHCO_3$, 0.3 Na_2HPO_4, 5 KCl, 0.3 KH_2PO_4, 1.25 $CaCl_2$, 0.5 $MgSO_4$, 0.5 $MgCl_2$, 5 HEPES, 22.2 glucose, and 0.001% (v/v) phenol red, with the pH adjusted to 7.2 using 0.3 N NaOH. *All*-trans retinal (1 μM) was added to the recording solution. The electrode solution contained the following (in mM): 110 Cs-Cl, 30 TEA-Cl, 2 $MgCl_2$, 0.1 $CaCl_2$, 10 EGTA, and 10 HEPES, with the pH adjusted to 7.25 using CsOH. Light stimuli were generated by 150-W xenon lamp-based scanning monochromators with a bandwidth of 10 nm (TILL Photonics, Germany). The light stimuli were coupled to the microscope with an optical fiber. The light intensity was attenuated with neutral density filters.

Animals and Viral Vector Injection

All animal experiments and procedures were approved by the Institutional Animal Care and Use Committee of Wayne State University, and they were performed in accordance with the NIH *Guide for the Care and Use of Laboratory Animals*. Intravitreal injections of the viral vectors were administered to at least 1-month-old wild-type C57BL/6J mice and $Opn4^{-/-}Gnat1^{-/-}Cnga3^{-/-}$ TKO transgenic mice. Briefly, the animal was anesthetized with an intraperitoneal

injection of a mixture of 100 mg kg^{-1} ketamine and 12 mg kg^{-1} xylazine. Viral vectors (1.5 μL) diluted in saline at a titer of 5×10^{12} vg/mL or vehicle (saline) were intravitreally injected into both eyes of each animal. The virus vectors were injected with a programmable Nanoliter Injector (Drummond Scientific, Broomall, PA, USA) using glass micropipettes. All experiments were performed at least 1 month after virus injection. Animals were euthanized by CO_2 asphyxiation followed by decapitation for electrophysiological recordings and immunostaining.

Immunostaining and Quantitative Cell Density Measurements

Enucleated eyes were fixed with 4% paraformaldehyde in phosphate buffer (PB) at room temperature for 20 min. Fluorescence expression was examined in flat-mounted retinas and retinal vertical sections. The expression of CoChR in RGCs was examined by co-labeling with mouse anti-GFP (1:1,000; Neuromab, UC Davis, Davis, CA, USA) and rabbit anti-RBPMS (1:1,000; ABN1362, Millipore Sigma, Temecula, CA, USA), an RGC-specific marker, antibodies. The secondary antibodies were conjugated to Alexa 555 (1:1,000) or Alexa 488 (1:600; Thermo Fisher Scientific, Waltham, MA, USA).

The densities of RGCs and CoChR-expressing RGCs were measured by assessing RBPMS-labeled and dual GFP/RBPMS-labeled cells, respectively. 3D z stack fluorescence images of the RGC layer in retinal whole mounts were captured using the Zeiss Apotome 2 Optical Photomicroscope (Carl Zeiss). The brightness and the contrast were adjusted. All quantifications of cell density were performed using ZEN software (Carl Zeiss). Eight images were captured in the middle regions of each retina (~1 mm from the optic disc) with the optimal exposure time. The cell numbers were manually counted with event tools in an area of 0.15 mm^2 of the original CZI (Carl Zeiss Image) file.

MEA Recordings

MEA recordings were performed using the previously described procedure.[6,56] Briefly, the retina was dissected and placed on a piece of nitrocellulose filter paper with the photoreceptor side down (Millipore, Bedford, MA, USA). The mounted retina was placed in the MEA-60 MEA recording chamber comprising 30-μm-diameter electrodes spaced 200 μm apart (Multi Channel System MCS, Reutlingen, Germany), with the ganglion cell layer facing the recording electrodes. The retina was continuously perfused with an oxygenated extracellular solution at 34°C during all experiments. The extracellular solution contained the following (in mM): 124 NaCl, 2.5 KCl, 2 $CaCl_2$, 2 $MgCl_2$, 1.25 NaH_2PO_4, 26 $NaHCO_3$, and 22 glucose (pH 7.35) with 95% O_2 and 5% CO_2. For C57BL/6J mice, the photoreceptor-mediated light responses were blocked with CNQX (50 μM), D-AP5 (20 μM), L-AP4 (20 μM), ACET (2 μM), DHβE (20 μM), bicuculline (50 μM), and strychnine (5 μM). For TKO mice, no photoreceptor-mediated light responses were observed under our light-adapted conditions, but L-AP4 and ACET were added to the solution in some recordings.

The interval between the onset of each light stimulus was 20 s. Signals were filtered between 200 Hz (low cutoff) and 20 kHz (high cutoff). A threshold of 24 μV was used to detect action potentials, and action potentials from individual neurons were determined with a standard expectation-maximization algorithm using offline Sorter software (Plexon, Dallas, TX, USA). The results were plotted using NeuroExplorer software (Nex Technologies, Madison, AL, USA). The relationship between the response-amplitude attenuation and frequency was measured from the averaged spike rate histograms. For each frequency, the attenuation was calculated by dividing the average trough-to-crest amplitude by the average peak amplitude. The attenuation values were converted to a decibel (dB) scale. Light stimuli were generated using 150-W xenon lamp-based scanning monochromators with a bandwidth of 10 nm (TILL Photonics, Germany). The light stimuli were directly projected onto the bottom of the recording chamber through an optical fiber. The light intensity was attenuated with neutral density filters.

Animal Behavioral Assays

OMRs were examined using a homemade optomotor system[38] and a commercially purchased OptoMotry system.[48] For the homemade optomotor system, the light illumination was provided by blue (a peak wavelength of ~470 nm), green (~520 nm), yellow (~590 nm), or natural white (4,500 K) LEDs. The light intensity of the LEDs was controlled by a digital power supply. The light intensities for monochromators and single-wavelength light (blue, green, and yellow LEDs) were presented as the unit of photons/cm^2s, whereas for natural white light (white LEDs) and the OptoMotry system they were presented as the unit of μW/cm^2. A positive OMR, or head tracking, was determined by repeated head angular movements in the direction of the rotating drum. Head tracking was tested for both clockwise and counterclockwise directions. Data obtained for the two directions of drum rotation from each animal were treated as two independent data points in the analysis. For the homemade system, the threshold light intensity at each grating frequency required to evoke OMR was determined. For the OptoMotry system, the procedures were the same as a previously published protocol.[48] The light intensity at the center of the platform was ~50 μW/cm^2. Visual acuity was measured in the OptoMotry system. It was defined as the highest grating frequency that can evoke animal head tracking at the grating contrast of 100% and the rotation speed of 12 d/s. The experimental data were confirmed by a second experimenter. All data are expressed as the mean ± SD, with "n" indicating the number of animals.

SUPPLEMENTAL INFORMATION

Supplemental Information can be found online at https://doi.org/10.1016/j.ymthe.2019.04.002.

AUTHOR CONTRIBUTIONS

T.H.G., Q.L., G.W.A., and Z.-H.P. designed the research. T.H.G. (Figure 1; Figures S1–S3; Table S1), Q.L. (Figures 2, 6, 7, and 8; Figure S4; Video S1), M.D.F. (Figures 6, 7, and 8), and Z.-H.P. (Figures 3, 4, 5, 6, 7, and 8; Video S1) performed experiments and analyzed data. Z.H.-P. with contributions from T.H.G., Q.L., and G.W.A. wrote the paper.

CONFLICTS OF INTEREST

T.H.G., Q.L., G.W.A., and Z.-H.P. are authors on a pending patent application related to this work filed by Wayne State University. M.D.F. declares no competing interests.

ACKNOWLEDGMENTS

This work was supported by the Ligon Research Center of Vision; the Kresge Eye Institute; the Dryer Foundation; an unrestricted departmental grant from Research to Prevent Blindness, Inc., (New York, NY, USA); and NIH (Bethesda, MD, USA), P30EY04068 to the Department of Ophthalmology, Visual and Anatomical Sciences at Wayne State University School of Medicine. We thank Andrea Krstevski for technical assistance.

REFERENCES

1. Hartong, D.T., Berson, E.L., and Dryja, T.P. (2006). Retinitis pigmentosa. Lancet *368*, 1795–1809.
2. de Jong, P.T. (2006). Age-related macular degeneration. N. Engl. J. Med. *355*, 1474–1485.
3. Busskamp, V., Picaud, S., Sahel, J.A., and Roska, B. (2012). Optogenetic therapy for retinitis pigmentosa. Gene Ther. *19*, 169–175.
4. Pan, Z.-H., Lu, Q., Bi, A., Dizhoor, A.M., and Abrams, G.W. (2015). Optogenetic approaches to restoring vision. Annu. Rev. Vis. Sci. *1*, 185–210.
5. Simunovic, M.P., Shen, W., Lin, J.Y., Protti, D.A., Lisowski, L., and Gillies, M.C. (2019). Optogenetic approaches to vision restoration. Exp. Eye Res. *178*, 15–26.
6. Bi, A., Cui, J., Ma, Y.P., Olshevskaya, E., Pu, M., Dizhoor, A.M., and Pan, Z.H. (2006). Ectopic expression of a microbial-type rhodopsin restores visual responses in mice with photoreceptor degeneration. Neuron *50*, 23–33.
7. Tomita, H., Sugano, E., Yawo, H., Ishizuka, T., Isago, H., Narikawa, S., Kügler, S., and Tamai, M. (2007). Restoration of visual response in aged dystrophic RCS rats using AAV-mediated channelopsin-2 gene transfer. Invest. Ophthalmol. Vis. Sci. *48*, 3821–3826.
8. Lin, B., Koizumi, A., Tanaka, N., Panda, S., and Masland, R.H. (2008). Restoration of visual function in retinal degeneration mice by ectopic expression of melanopsin. Proc. Natl. Acad. Sci. USA *105*, 16009–16014.
9. Lagali, P.S., Balya, D., Awatramani, G.B., Münch, T.A., Kim, D.S., Busskamp, V., Cepko, C.L., and Roska, B. (2008). Light-activated channels targeted to ON bipolar cells restore visual function in retinal degeneration. Nat. Neurosci. *11*, 667–675.
10. Busskamp, V., Duebel, J., Balya, D., Fradot, M., Viney, T.J., Siegert, S., Groner, A.C., Cabuy, E., Forster, V., Seeliger, M., et al. (2010). Genetic reactivation of cone photoreceptors restores visual responses in retinitis pigmentosa. Science *329*, 413–417.
11. Doroudchi, M.M., Greenberg, K.P., Liu, J., Silka, K.A., Boyden, E.S., Lockridge, J.A., Arman, A.C., Janani, R., Boye, S.E., Boye, S.L., et al. (2011). Virally delivered channelrhodopsin-2 safely and effectively restores visual function in multiple mouse models of blindness. Mol. Ther. *19*, 1220–1229.
12. Tomita, H., Sugano, E., Murayama, N., Ozaki, T., Nishiyama, F., Tabata, K., Takahashi, M., Saito, T., and Tamai, M. (2014). Restoration of the majority of the visual spectrum by using modified Volvox channelrhodopsin-1. Mol. Ther. *22*, 1434–1440.
13. Cronin, T., Vandenberghe, L.H., Hantz, P., Juttner, J., Reimann, A., Kacsó, A.E., Huckfeldt, R.M., Busskamp, V., Kohler, H., Lagali, P.S., et al. (2014). Efficient transduction and optogenetic stimulation of retinal bipolar cells by a synthetic adeno-associated virus capsid and promoter. EMBO Mol. Med. *6*, 1175–1190.
14. Macé, E., Caplette, R., Marre, O., Sengupta, A., Chaffiol, A., Barbe, P., Desrosiers, M., Bamberg, E., Sahel, J.A., Picaud, S., et al. (2015). Targeting channelrhodopsin-2 to ON-bipolar cells with vitreally administered AAV Restores ON and OFF visual responses in blind mice. Mol. Ther. *23*, 7–16.
15. Gaub, B.M., Berry, M.H., Holt, A.E., Isacoff, E.Y., and Flannery, J.G. (2015). Optogenetic Vision Restoration Using Rhodopsin for Enhanced Sensitivity. Mol. Ther. *23*, 1562–1571.
16. Cehajic-Kapetanovic, J., Eleftheriou, C., Allen, A.E., Milosavljevic, N., Pienaar, A., Bedford, R., Davis, K.E., Bishop, P.N., and Lucas, R.J. (2015). Restoration of Vision with Ectopic Expression of Human Rod Opsin. Curr. Biol. *25*, 2111–2122.
17. van Wyk, M., Pielecka-Fortuna, J., Löwel, S., and Kleinlogel, S. (2015). Restoring the ON Switch in Blind Retinas: Opto-mGluR6, a Next-Generation, Cell-Tailored Optogenetic Tool. PLoS Biol. *13*, e1002143.
18. Sengupta, A., Chaffiol, A., Macé, E., Caplette, R., Desrosiers, M., Lampič, M., Forster, V., Marre, O., Lin, J.Y., Sahel, J.A., et al. (2016). Red-shifted channelrhodopsin stimulation restores light responses in blind mice, macaque retina, and human retina. EMBO Mol. Med. *8*, 1248–1264.
19. Thompson, D.A., and Gal, A. (2003). Vitamin A metabolism in the retinal pigment epithelium: genes, mutations, and diseases. Prog. Retin. Eye Res. *22*, 683–703.
20. Nagel, G., Ollig, D., Fuhrmann, M., Kateriya, S., Musti, A.M., Bamberg, E., and Hegemann, P. (2002). Channelrhodopsin-1: a light-gated proton channel in green algae. Science *296*, 2395–2398.
21. Nagel, G., Szellas, T., Huhn, W., Kateriya, S., Adeishvili, N., Berthold, P., Ollig, D., Hegemann, P., and Bamberg, E. (2003). Channelrhodopsin-2, a directly light-gated cation-selective membrane channel. Proc. Natl. Acad. Sci. USA *100*, 13940–13945.
22. Nagel, G., Brauner, M., Liewald, J.F., Adeishvili, N., Bamberg, E., and Gottschalk, A. (2005). Light activation of channelrhodopsin-2 in excitable cells of Caenorhabditis elegans triggers rapid behavioral responses. Curr. Biol. *15*, 2279–2284.
23. Zhang, F., Prigge, M., Beyrière, F., Tsunoda, S.P., Mattis, J., Yizhar, O., Hegemann, P., and Deisseroth, K. (2008). Red-shifted optogenetic excitation: a tool for fast neural control derived from *Volvox carteri*. Nat. Neurosci. *11*, 631–633.
24. Lin, J.Y., Lin, M.Z., Steinbach, P., and Tsien, R.Y. (2009). Characterization of engineered channelrhodopsin variants with improved properties and kinetics. Biophys. J. *96*, 1803–1814.
25. Wen, L., Wang, H., Tanimoto, S., Egawa, R., Matsuzaka, Y., Mushiake, H., Ishizuka, T., and Yawo, H. (2010). Opto-current-clamp actuation of cortical neurons using a strategically designed channelrhodopsin. PLoS ONE *5*, e12893.
26. Berndt, A., Schoenenberger, P., Mattis, J., Tye, K.M., Deisseroth, K., Hegemann, P., and Oertner, T.G. (2011). High-efficiency channelrhodopsins for fast neuronal stimulation at low light levels. Proc. Natl. Acad. Sci. USA *108*, 7595–7600.
27. Kleinlogel, S., Feldbauer, K., Dempski, R.E., Fotis, H., Wood, P.G., Bamann, C., and Bamberg, E. (2011). Ultra light-sensitive and fast neuronal activation with the Ca^2+-permeable channelrhodopsin CatCh. Nat. Neurosci. *14*, 513–518.
28. Prigge, M., Schneider, F., Tsunoda, S.P., Shilyansky, C., Wietek, J., Deisseroth, K., and Hegemann, P. (2012). Color-tuned channelrhodopsins for multiwavelength optogenetics. J. Biol. Chem. *287*, 31804–31812.
29. Lin, J.Y., Knutsen, P.M., Muller, A., Kleinfeld, D., and Tsien, R.Y. (2013). ReaChR: a red-shifted variant of channelrhodopsin enables deep transcranial optogenetic excitation. Nat. Neurosci. *16*, 1499–1508.
30. Pan, Z.-H., Ganjawala, T.H., Lu, Q., Ivanova, E., and Zhang, Z. (2014). ChR2 mutants at L132 and T159 with improved operational light sensitivity for vision restoration. PLoS ONE *9*, e98924.
31. Klapoetke, N.C., Murata, Y., Kim, S.S., Pulver, S.R., Birdsey-Benson, A., Cho, Y.K., Morimoto, T.K., Chuong, A.S., Carpenter, E.J., Tian, Z., et al. (2014). Independent optical excitation of distinct neural populations. Nat. Methods *11*, 338–346.
32. Wietek, J., Wiegert, J.S., Adeishvili, N., Schneider, F., Watanabe, H., Tsunoda, S.P., Vogt, A., Elstner, M., Oertner, T.G., and Hegemann, P. (2014). Conversion of channelrhodopsin into a light-gated chloride channel. Science *344*, 409–412.
33. Govorunova, E.G., Sineshchekov, O.A., Janz, R., Liu, X., and Spudich, J.L. (2015). NEUROSCIENCE. Natural light-gated anion channels: A family of microbial rhodopsins for advanced optogenetics. Science *349*, 647–650.
34. Zhang, Y., Ivanova, E., Bi, A., and Pan, Z.-H. (2009). Ectopic expression of multiple microbial rhodopsins restores ON and OFF light responses in retinas with photoreceptor degeneration. J. Neurosci. *29*, 9186–9196.
35. Greenberg, K.P., Pham, A., and Werblin, F.S. (2011). Differential targeting of optical neuromodulators to ganglion cell soma and dendrites allows dynamic control of center-surround antagonism. Neuron *69*, 713–720.
36. Wu, C., Ivanova, E., Zhang, Y., and Pan, Z.-H. (2013). rAAV-mediated subcellular targeting of optogenetic tools in retinal ganglion cells in vivo. PLoS ONE *8*, e66332.

37. Chaffiol, A., Caplette, R., Jaillard, C., Brazhnikova, E., Desrosiers, M., Dubus, E., Duhamel, L., Macé, E., Marre, O., Benoit, P., et al. (2017). A New Promoter Allows Optogenetic Vision Restoration with Enhanced Sensitivity in Macaque Retina. Mol. Ther. *25*, 2546–2560.

38. Lu, Q., Ganjawala, T.H., Hattar, S., Abrams, G.W., and Pan, Z.-H. (2018). A Robust optomotor assay for assessing the efficacy of optogenetic tools for vision restoration. Invest. Ophthalmol. Vis. Sci. *59*, 1288–1294.

39. Mattis, J., Tye, K.M., Ferenczi, E.A., Ramakrishnan, C., O'Shea, D.J., Prakash, R., Gunaydin, L.A., Hyun, M., Fenno, L.E., Gradinaru, V., et al. (2011). Principles for applying optogenetic tools derived from direct comparative analysis of microbial opsins. Nat. Methods *9*, 159–172.

40. Hart, W.M., Jr. (1987). The temporal responsiveness of vision. In Adler's Physiology of the Eye: Clinical Application, 8th Edition, R.A. Moses and W.M. Hart, eds. (St. Louis, MO: The C.V. Mosby Company), pp. 429–457.

41. Schild, L.C., and Glauser, D.A. (2015). Dual color neural activation and behavior control with chrimson and CoChR in caenorhabditis elegans. Genetics *200*, 1029–1034.

42. Shemesh, O.A., Tanese, D., Zampini, V., Linghu, C., Piatkevich, K., Ronzitti, E., Papagiakoumou, E., Boyden, E.S., and Emiliani, V. (2017). Temporally precise single-cell-resolution optogenetics. Nat. Neurosci. *20*, 1796–1806.

43. Berndt, A., Yizhar, O., Gunaydin, L.A., Hegemann, P., and Deisseroth, K. (2009). Bistable neural state switches. Nat. Neurosci. *12*, 229–234.

44. Dawydow, A., Gueta, R., Ljaschenko, D., Ullrich, S., Hermann, M., Ehmann, N., Gao, S., Fiala, A., Langenhan, T., Nagel, G., and Kittel, R.J. (2014). Channelrhodopsin-2-XXL, a powerful optogenetic tool for low-light applications. Proc. Natl. Acad. Sci. USA *111*, 13972–13977.

45. Vincent, M.J., Martin, A.S., and Compans, R.W. (1998). Function of the KKXX motif in endoplasmic reticulum retrieval of a transmembrane protein depends on the length and structure of the cytoplasmic domain. J. Biol. Chem. *273*, 950–956.

46. Doi, S., Tsukamoto, T., Yoshizawa, S., and Sudo, Y. (2017). An inhibitory role of Arg-84 in anion channelrhodopsin-2 expressed in Escherichia coli. Sci. Rep. *7*, 41879.

47. Hattar, S., Lucas, R.J., Mrosovsky, N., Thompson, S., Douglas, R.H., Hankins, M.W., Lem, J., Biel, M., Hofmann, F., Foster, R.G., and Yau, K.W. (2003). Melanopsin and rod-cone photoreceptive systems account for all major accessory visual functions in mice. Nature *424*, 76–81.

48. Prusky, G.T., Alam, N.M., Beekman, S., and Douglas, R.M. (2004). Rapid quantification of adult and developing mouse spatial vision using a virtual optomotor system. Invest. Ophthalmol. Vis. Sci. *45*, 4611–4616.

49. Dillon, J., Zheng, L., Merriam, J.C., and Gaillard, E.R. (1999). The optical properties of the anterior segment of the eye: implications for cortical cataract. Exp. Eye Res. *68*, 785–795.

50. Lei, B., and Yao, G. (2006). Spectral attenuation of the mouse, rat, pig and human lenses from wavelengths 360 nm to 1020 nm. Exp. Eye Res. *83*, 610–614.

51. Henriksson, J.T., Bergmanson, J.P., and Walsh, J.E. (2010). Ultraviolet radiation transmittance of the mouse eye and its individual media components. Exp. Eye Res. *90*, 382–387.

52. Umino, Y., Solessio, E., and Barlow, R.B. (2008). Speed, spatial, and temporal tuning of rod and cone vision in mouse. J. Neurosci. *28*, 189–198.

53. Kuffler, S.W. (1953). Discharge patterns and functional organization of mammalian retina. J. Neurophysiol. *16*, 37–68.

54. Enroth-Cugell, C., and Robson, J.G. (1966). The contrast sensitivity of retinal ganglion cells of the cat. J. Physiol. *187*, 517–552.

55. Baker, C.K., and Flannery, J.G. (2018). Innovative Optogenetic Strategies for Vision Restoration. Front. Cell. Neurosci. *12*, 316.

56. Tian, N., and Copenhagen, D.R. (2003). Visual stimulation is required for refinement of ON and OFF pathways in postnatal retina. Neuron *39*, 85–96.

YMTHE, Volume *27*

Supplemental Information

Improved CoChR Variants Restore Visual Acuity and Contrast Sensitivity in a Mouse Model of Blindness under Ambient Light Conditions

Tushar H. Ganjawala, Qi Lu, Mitchell D. Fenner, Gary W. Abrams, and Zhuo-Hua Pan

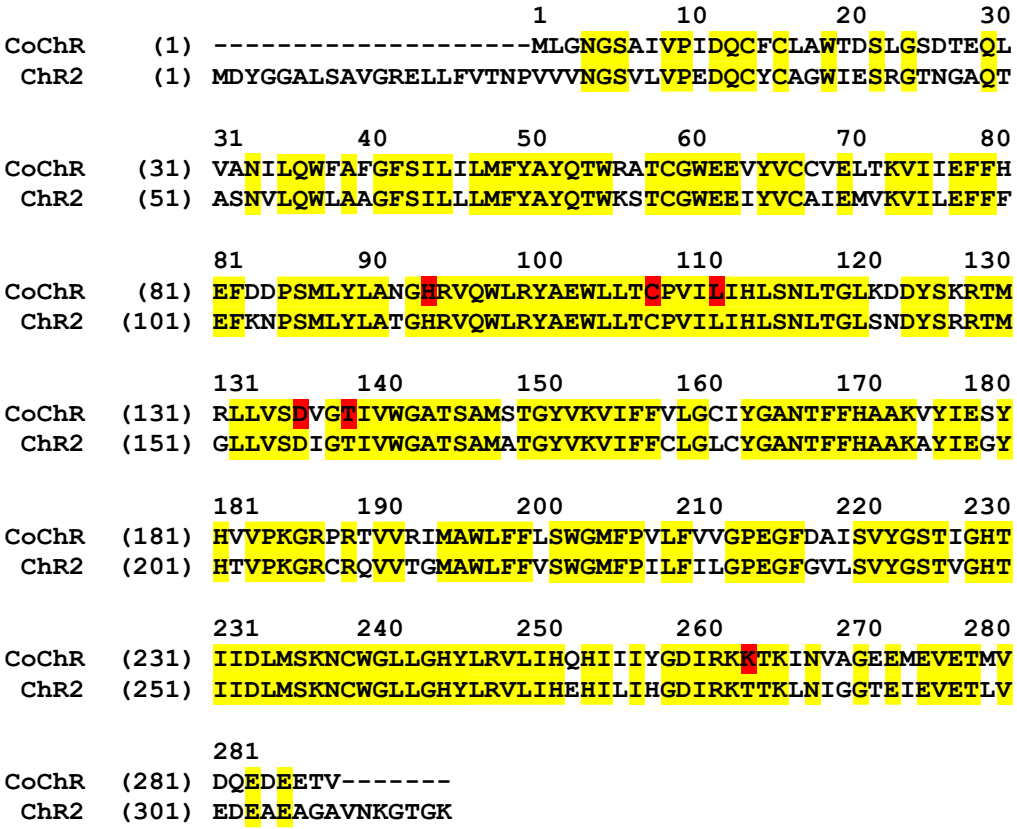

Figure S1. Alignment of the amino acid sequences of ChR2 and CoChR
The labeled amino acids are for CoChR. The conserved amino acids are highlighted in yellow. The mutated amino acids in CoChR reported in this study are highlighted in red.

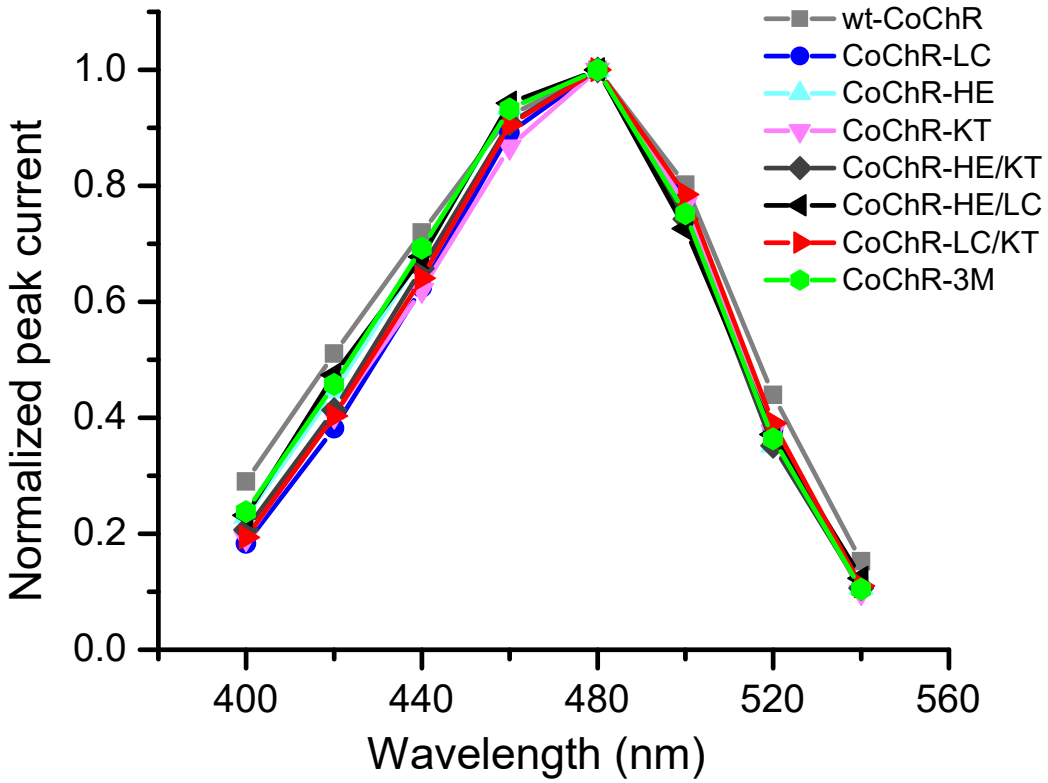

Figure S2. Comparison of the spectral properties of wt-CoChR and CoChR mutants in HEK cells

Photocurrents were elicited by 1-s light pulses of different wavelengths with a ND filter of 2.5. The spectral curves are normalized to the peak photocurrents. The data for each mutant are the average of 3 cells.

Table S1. Off-rates and peak current amplitudes for wt-CoChR and CoChR mutants examined in HEK cells

CoChR mutants	Off rate (ms) mean ± SEM	Current (pA) mean ± SEM	*n*
Wild type	112 ± 11	368 ± 44	10
L112C	372 ± 56	593 ± 91	10
L112A	1429 ± 170	707 ± 183	6
L112D*	nd	33 ± 7	5
L112S	1433 ± 96	474 ± 71	3
T139C	292 ± 33	393 ± 77	7
T139A	2109 ± 449	452 ± 131	7
T139S	671 ± 59	354 ± 118	6
L112C-T139C	751 ± 102	577 ± 123	6
C108A*	No deactivation	152 ± 4	3
C108T*	903 ± 180	52 ± 13	3
D136A*	nd	nd	3
D136C*	nd	39 ± 25	3
D136T*	nd	nd	2
K264T	186 ± 18	640 ± 90	10
H94E	174 ± 12	388 ± 42	10
H95E-K264T	133 ± 12	212 ± 35	11
H94E-L112C	614 ± 46	618 ± 80	10
L112C-K264T	376 ± 36	516 ± 65	13
H94E-L112C-K264T	723 ± 71	955 ± 87	10

Mutants noted with an asterisk exhibited notable aggregation. nd: not determined.

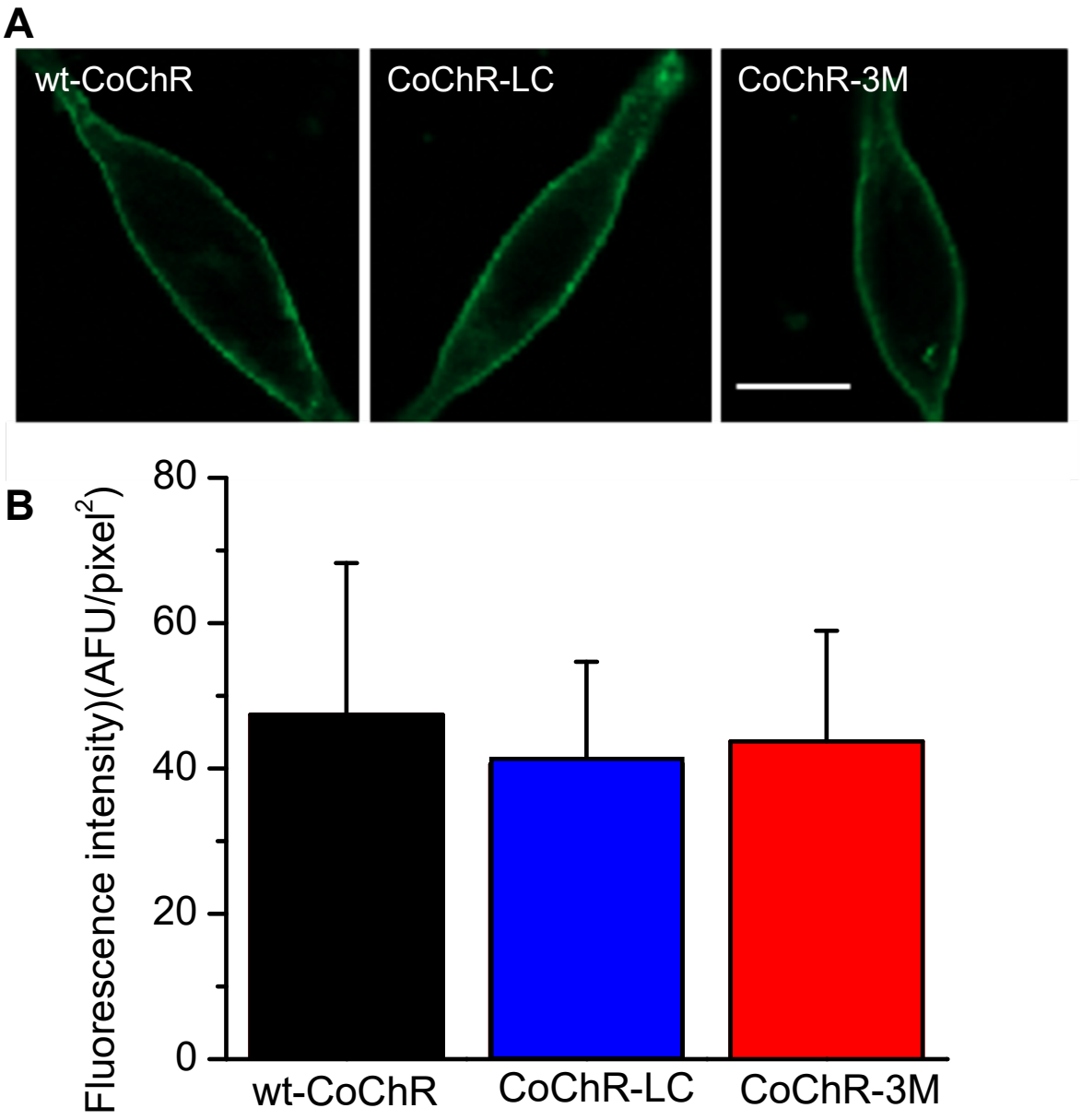

Figure S3. Comparison of the membrane expression efficiencies of CoChRs in HEK cells

(A) Representative images showing the expression of ChR-GFP for wt-CoChR, CoChR-LC, and CoChR-3M. Scale bar, 10 μm. (B) Fluorescence intensities measured in the plasma membrane region. The data are shown in arbitrary fluorescence units (AFU/pixel^2) (means ± SD; n = 29 – 38 cells).

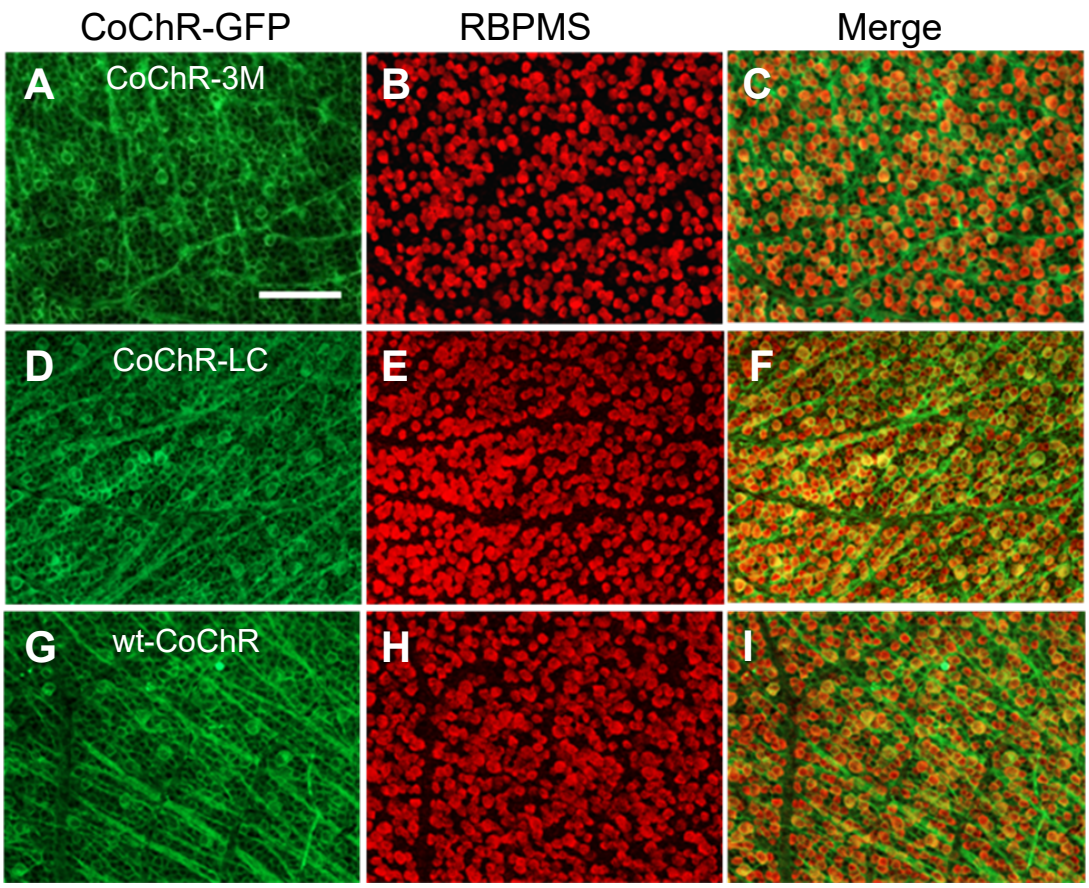

Figure S4. Expression of CoChR-GFP in TKO mouse retinas *in vivo*
Representative immunofluorescence images showing co-labeling of GFP with RBPMS in retinal whole mounts for CoChR-3M (A–C), CoChR-L112C (D–F), wt-CoChR (G–I). Scale bar, 100 μm.